TURBULENT DISPERSION IN CLOUDY BOUNDARY LAYERS

Remco Verzijlbergh, Harm J. J. Jonker*, Thijs Heus
Multi-Scale Physics, Delft University of Technology, The Netherlands

ABSTRACT

Compared to dry boundary layers, dispersion in cloud-topped boundary layers seems to have received less attention. In this LES based numerical study we investigate the dispersion of a passive tracer in the form of Lagrangian particles for four kinds of atmospheric boundary layers: 1) a dry convective boundary layer (for reference), 2) a 'smoke' cloud boundary layer in which the turbulence is driven by radiative cooling, 3) a stratocumulus topped boundary layer and 4) a shallow cumulus topped boundary layer.

We show that the dispersion characteristics of the smoke cloud boundary layer as well as the stratocumulus situation can be well understood by borrowing concepts from the dry convective boundary layer. A general result is that the presence of clouds enhances mixing and dispersion – a notion that is not always reflected well in traditional parameterization models, in which clouds usually suppress dispersion by diminishing solar irradiance.

The dispersion characteristics of a cumulus cloud layer turn out to be markedly different from the other three cases and the results can not be explained by only considering the well-known top-hat velocity distribution. To understand the surprising behaviour in the shallow cumulus layer, this case has been examined in more detail by 1) determining the velocity distribution conditioned on the distance to the nearest cloud and 2) accounting for the wavelike behaviour associated with the stratified dry environment.

1. INTRODUCTION

This paper describes the dispersion of a passive tracer in different types of atmospheric boundary layers with emphasis on the dispersion in cloudy boundary layers. As we discuss below, understanding the diffusion of pollutants in cloudy boundary layers is important for climate, air quality and atmospheric chemistry.

Clouds are known to transport pollutants from the boundary layer to higher regions in the atmosphere, a phenomenon referred to as cloud venting (e.g. Cotton (1995)). Interestingly, the relationship between particles in the atmosphere and clouds works both ways: not only do clouds deposit pollutants (gases, aerosols) in the atmosphere, they are also strongly influenced by them. The optical properties as well as the lifetime of a cloud are known to depend on the aerosol distribution in the cloud's environment. On the other hand, both the optical properties of clouds as well as their lifetimes affect the earth's radiation budget and hence global climate.

Chemical processes in the atmosphere are also influenced by clouds. First of all they affect transport of chemical compounds through the atmosphere and enhance turbulent mixing of different species. In addition clouds can alter the photodissociation rates of chemical compounds around them (Vilà-Guerau de Arellano et al., 2005).

Finally, next to the importance of dispersion on climate and atmospheric chemistry, ground level concentrations of pollutants are also influenced by the meteorological conditions they were emitted in. The classical work relating dispersion and turbulence was done by Taylor (1921). This analysis, however, was based on homogeneous turbulence, whereas atmospheric motions are often very complex and characterized by non-homogeneous turbulence. Pasquill (1961) proposed a Gaussian plume model with a vertical dispersion coefficient depending on the meteorological circumstances. Basically, the vertical dispersion coefficient is then related to the stability of the atmosphere, which is related to the amount of insolation. In this view, clouds have a damping effect on dispersion in daytime conditions.

The subject of atmospheric dispersion has been further extensively studied in laboratory, field experiments and by numerical methods. The pioneering water tank experiments of Willis and Deardorff (1978) demonstrated the effects of the non-homogeneous turbulence of a convective boundary layer (CBL) on diffusion of particles. They showed, rather surprisingly at the time, that a near-ground release resulted in a quickly rising plume (in terms of the peak concentration), but an elevated release resulted in a descending plume that only rises after impinging on the ground. The water tank results have also been verified by full-scale atmospheric experiments (Briggs, 1993). Lamb (1978) used the velocity fields from Large Eddy Simulations to investigate dispersion of particles. Nieuwstadt (1992) used the advection of a passive scalar in an LES model to describe the dispersion of a line source in the dry CBL. More recently Dosio and Vilà-Guerau de Arellano (2006) gave a thorough statistical description of dispersion in the dry CBL in an LES based study. An LES study of dispersion in a stable boundary layer was recently conducted by e.g. Weil et al. (2006).

In contrast with the number of studies on dispersion in the CBL is the modest number of studies on dispersion in cloudy boundary layers. Some field experiments have demonstrated the effect of cloud venting (e.g. Ching et al. (1988), Angevine (2005)). Vilà-Guerau de Arellano et al. (2005) have shown in a LES study how shallow cumulus enhance vertical transport of pollutants, thereby specifi-

* *Corresponding author address:* Harm Jonker, Dept. of Multi-Scale Physics, Delft University of Technology, Delft, The Netherlands (h.j.j.jonker@tudelft.nl - www.msp.tudelft.nl)

cally focussing on the influence on chemical transformations. Weil et al. (1993) used ice-crystals as a tracer to study relative dispersion in an ensemble of cumulus clouds.

Because a comprehensive study of dispersion in cloudy boundary layers appears to be missing, the objective of this study is to investigate and statistically describe turbulent dispersion in different types of cloudy boundary layers. To this end we perform large eddy simulations together with a Lagrangian particle module. Four types of boundary layers will be considered: the clear convective boundary layer, the smoke cloud boundary layer, the stratocumulus topped boundary layer and finally the shallow cumulus topped boundary layer. The differences and similarities between these four atmospheric situations offer a nice opportunity to gain more insight in the observed dispersion characteristics. In section 2 we describe the methodology consisting of the numerical setup, the case characteristics and the definition of statistical quantities. Section 3, in which the results are presented and discussed, is divided into two parts: a phenomenological part with a qualitative description of the dispersion characteristics in the different boundary layers is followed by a more quantitative part.

2. METHODOLOGY

2.1 *LES model and Lagrangian particle dispersion model*

The LES-code used in this research is version 3 of the Dutch Atmospheric LES (DALES3) as described by Cuijpers and Duynkerke (1993). In this study, Lagrangian particles rather than a concentration field of a scalar are used as a representation of the pollutants. To this end, a Lagrangian Particle Dispersion Module (LPDM) as described in Heus et al. (2008) is implemented in the LES. This LPDM is largely based on the criteria for stochastic Lagrangian models formulated by Thomson (1987). The implementation of these criteria in LES models described in Weil et al. (2004) is followed in the present LPDM. Using Lagrangian particles has the advantage of being able to track individual particles in time, thereby allowing the calculation of Lagrangian statistics. Contrary to Nieuwstadt (1992) and Dosio and Vilà-Guerau de Arellano (2006), an instantaneous plane source rather than an instantaneous line source is used in this study. We can view the plane source of $1024^2 \approx 1 \times 10^6$ particles homogeneously distributed over the domain in both horizontal directions as a collection of 1024 linesources. Details about the numerics of the simulations vary between the different cases and will be discussed in the next section.

2.2 *Case descriptions*

Hereafter we describe briefly the four different atmospheric situations that have been under consideration. Numerical values of the case characteristics are listed in table 1. Figure 2 shows the profiles of the virtual potential temperature flux $\langle\overline{w'\theta_v'}\rangle$. These profiles give an indication about the dynamics and the structure of the boundary layer.

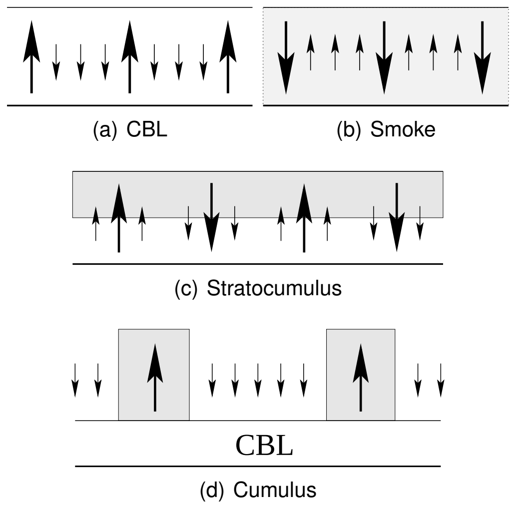

FIG. 1: Conceptual representation of the velocity distributions in the different boundary layers.

Dry convective boundary layer The CBL is characterized by a well mixed layer, a strong surface heat flux and a capping inversion. This gives rise to a positively skewed velocity distribution: strong localized updrafts surrounded by moderate compensating downdrafts, as depicted schematically in figure 1(a). Figure 2(a) shows the buoyancy flux profile for the CBL. It must be noted that although the initial boundary layer height was at $900m$ as given in table 1, entrainment increased the boundary layer height already till somewhat above this value. The simulation was run on a grid of 256^3 points, with a horizontal resolution of $\Delta x = \Delta y = 25\,\mathrm{m}$ and a vertical of $\Delta z = 6\,\mathrm{m}$, resulting in a domain of $6.4\,\mathrm{km} \times 6.4\,\mathrm{km} \times 1.5\,\mathrm{km}$. A timestep of $\Delta t = 1\,\mathrm{s}$ and a 5^{th} order advection scheme have been used, except for the advection of momentum, for which a centred-difference scheme has been used. The particles were released after three hours of simulation.

Smoke cloud boundary layer The smoke case used in this study is described in an intercomparison study by Bretherton et al. (1999). The smoke case is particularly useful to gain understanding of the stratocumulus case, for it has the same radiation characteristics, but there are no condensation or surface fluxes to additionally drive convection. Making the analogy with the CBL, instead of heating at the bottom (CBL) we have radiative cooling at the top (Smoke). This results in a mirror image of the vertical velocity distribution from the CBL, as depicted in figure 1(b)

Figure 2(b) shows the buoyancy flux in the smoke cloud. Next to the absence of a surface heat flux, we also observe entrainment at the top of the smoke cloud.

	z_i	$\langle\overline{w'q_t'}\rangle_0$	$\langle\overline{w'\theta_l'}\rangle_0$	w_*	t_*
dry CBL	900	0	9.4×10^{-2}	1.42	633
smoke	700	0	0	0.92	760
stratocumulus	700	1×10^{-5}	1×10^{-2}	0.87	804
shallow cumulus	2000	1.2×10^{-4}	1.5×10^{-2}	1.66	1204

Table 1: Characteristics of the different cases: the approximate boundary layer height z_i at the moment of particle release, the surface moisture and heat fluxes $\langle\overline{w'q_t'}\rangle_0$ and $\langle\overline{w'\theta_l'}\rangle_0$, the characteristic velocity scale w_* as defined in equation 2, the characteristic timescale t_*.

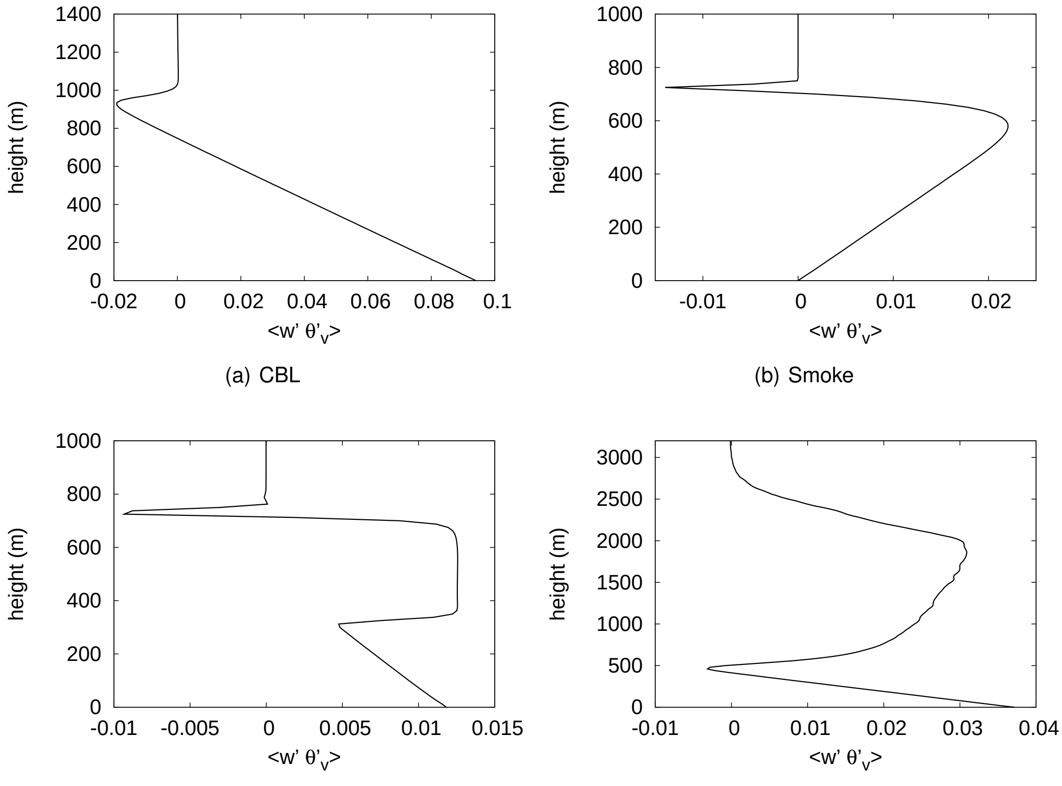

(a) CBL

(b) Smoke

(c) Stratocumulus

(d) Cumulus

FIG. 2: Virtual potential temperature flux $\langle\overline{w'\theta_v'}\rangle$ in the four different boundary layers

In the smoke case the domain measured $3.2\,\mathrm{km} \times 3.2\,\mathrm{km} \times 1.2\,\mathrm{km}$. Horizontal and vertical resolutions are $\Delta x = \Delta y = 12.5\,\mathrm{m}$ and $\Delta z = 6.25\,\mathrm{m}$ and the number of grid points is 256 in the horizontal and 200 in the vertical direction. For the scalar variables the kappa advection scheme (Hundsdorfer et al., 1995) and for momentum the centred-differences scheme with a timestep of $\Delta t = 0.5\,\mathrm{s}$ have been used. The particles were released after two hours of simulation.

Stratocumulus topped boundary layer The stratocumulus case under consideration is the Atlantic Stratocumulus Transition Experiment (ASTEX, de Roode and Duynkerke (1997)). Data from flight 2, A209, has been used. Convection in a stratocumulus topped boundary layer is driven by a combination of processes: radiative cooling at cloudtop, surface fluxes of heat and moisture and latent heat release due to condensation. In analogy with the previous cases, in terms of the driving mechanisms, the stratocumulus case can be considered a combination of the CBL and the smoke cloud. This translates into a velocity distribution that is a combination of the CBL and the smoke case, thus giving rise to a more symmetric velocity distribution, as depicted in figure 1(c).

Figure 2(c) shows the virtual potential temperature flux of the stratocumulus case. We already stated that the stratocumulus is a combination of the CBL and the smoke case, but here we specify that it is especially in the cloud layer (starting at approximately 350m) that the smoke cloud characteristics are found. In the subcloud layer, the profile looks more like that in the CBL.

The numerical grid in the stratocumulus case consists of 256^3 points with a horizontal resolution of $\Delta x = \Delta y = 25\,\mathrm{m}$ and a vertical resolution of $\Delta z = 6.25\,\mathrm{m}$, spanning a domain of $6.4\,\mathrm{km} \times 6.4\,\mathrm{km} \times 1.6\,\mathrm{km}$. Like the smoke case, the kappa advection scheme for scalars and centred-differences for momentum with a timestep of $\Delta t = 0.5\,\mathrm{s}$ have been used. After two hours, regarded as spin-up period, the particles were released.

Shallow cumulus topped boundary layer The shallow cumulus (in the remainder of the article referred to as cumulus) case used in this study is derived from the Small Cumulus Microphysics Study (SCMS) as described in Neggers et al. (2003) The cumulus topped boundary layer can be considered as two layers on top of each other. The subcloud layer has the characteristics of a dry CBL. The velocity distribution in the cloud layer is often thought and also parametrized (Siebesma and Cuijpers, 1995) as positively skewed: strong localized updrafts in the cloudy regions and homogeneously distributed compensating downdrafts elsewhere, see figure 1(d). Recent studies by Heus and Jonker (2008) and Jonker et al. (2008) have however shown that downward mass transport occurs mainly near the edge of a cloud, a mechanism referred to as the subsiding shell.

From the buoyancy flux profile, figure 3(d), it can be seen that cloud base is located at approximately $500m$ and the cloud layer extends to $2500m$. The subcloud layer has a profile similar to the CBL.

Numerical resolutions in the cumulus case are $\Delta x = \Delta y = 25\,\mathrm{m}$ in the horizontal and $\Delta z = 20\,\mathrm{m}$ in the vertical. With 256^3 points, this amounts to a domain of $6.4\,\mathrm{km} \times 6.4\,\mathrm{km} \times 5.2\,\mathrm{km}$. A centered-difference integration scheme with a timestep of $\Delta t = 1\,\mathrm{s}$ has been used. The particles were released after three hours of spin-up, allowing for a fully developed cumulus field.

2.3 *Scaling parameters*

In order to compare the results of the different boundary layers, we introduce the following dimensionless velocity and timescales. For the CBL, the following well known convective velocity scale is often used

$$w_* = \left(\frac{g}{\theta_0} \overline{(w'\theta_v')_0} z_i \right)^{1/3} \tag{1}$$

The velocity scales in the stratocumulus and the smoke case are calculated, following de Roode and Duynkerke (1997), according to

$$w_* = \left(c_1 \frac{g}{\theta_0} \int_0^{L_z} \overline{w'\theta_v} dz \right)^{1/3} \tag{2}$$

where the factor c_1 has the value 2.5 and L_z is the domain height. The value of c_1 is derived by Deardorff (1980) in order to make Eq. 2 consistent with Eq. 1. We suggest to use equation 2 also for the cumulus case. This makes sense from a physical point of view , since the integral in Eq. 2 represents the production of turbulent kinetic energy. Furthermore, it is the most consistent choice, since we can now use Eq. 2 for all the cases under consideration. Although in the definition by Deardorff (1980) the integration is till the inversion height, we integrate over the entire domain because in the cumulus case the definition of the inversion height is not so clear. Concerning the other cases, since there is hardly any buoyancy flux above the inversion height, replacing z_i by L_z in Eq. 2 leads only to a very small difference.

For each case we take for the dimensionless time

$$t_* = \frac{z_i}{w_*} \tag{3}$$

2.4 *Statistics*

In this section we introduce the statistical variables necessary to adequately describe the dispersion characteristics. The instantaneous concentration $c(x, y, z, t)$ of particles is computed by counting the number of particles N_p in a small box $\Delta V = \Delta x \Delta y \Delta z$ centered at (x, y, z). This value is divided by the total number of particles N_{tot} so that we have a normalized concentration:

$$c(x, y, z, t) = \frac{N_p(x, y, z, t)}{N_{tot} \Delta x \Delta y \Delta z} \tag{4}$$

$$\int_V c \; dx \; dy \; dz = 1 \tag{5}$$

The various statistical parameters can now be defined. The first statistical moment or mean plume height is given by

$$\overline{z} = \int_V zc\, dx\, dy\, dz \tag{6}$$

The vertical dispersion coefficient is defined by

$$\sigma_z^2 = \int_V (z - \overline{z})^2 c\, dx\, dy\, dz \tag{7}$$

where the difference with the mean plume height is used rather than the source height. For the skewness of the plume we get

$$S_z = \frac{1}{\sigma_z^3} \int_V (z - \overline{z})^3 c\, dx\, dy\, dz \tag{8}$$

Another useful quantity is the horizontally integrated concentration, that we will call the vertical concentration profile

$$C_z(z,t) = \frac{1}{A} \int_A c\, dx\, dy \tag{9}$$

Equivalently we define a horizontal concentration profile according to

$$C_y(y,t) = \frac{1}{A_{xz}} \int_{A_{xz}} c\, dx\, dz \tag{10}$$

were $A_{xz} = L_x L_z$ is a vertical cross-section of the domain, L_z denoting the domain height.

2.5 *Velocity statistics*

Next to the probability density function (PDF) of vertical velocity we shall consider the Lagrangian velocity autocorrelation function, defined by

$$R_u^L = \frac{\overline{u'(t)u'(t+\tau)}}{\sigma_u^2} \tag{11}$$

with $u_i'(t) = u_i(t) - \overline{u_i(t)}$ the velocity fluctuation of the i^{th} particle and the overbar represents the average over all particles and u can be u, v, w.

3. RESULTS AND DISCUSSION

3.1 *Plume phenomenology for different types of boundary layers.*

To give a first general impression of the dispersion characteristics of the four different boundary layers, the time evolution of the concentration profiles are depicted in figure 3. For all the cases, $1024^2 \approx 1 \times 10^6$ particles were released instantaneously in a horizontal plane at half the boundary layer height, 2 or 3 hours, depending on the case, after the start of the simulation to allow for the spin-up. We briefly discuss the general features of Fig. 3. In the next section we will go into more detail for each case individually.

The evolution of the plume in the CBL, figure 3(a), has the familiar shape that was described by Willis and Deardorff (1978): the plume concentration maximum initially descends to the ground, stays there for a while and then rises again until the plume is entirely mixed. After 3 turnover times the particles are almost homogeneously distributed throughout the boundary layer. The initial descent of the plume can be explained from the skewness of the vertical velocity distribution, as shown in figure 1(a).

The plume evolution in the smoke cloud boundary layer looks at first sight as a reversed version of what happens in the dry CBL. The plume maximum rises till it reaches the inversion, remains there some time and descends again. The observed plume can again be understood by considering the skewness of the vertical velocity distribution as depicted in figure 1(b).

The plume evolution in the stratocumulus topped boundary layer is, at least for short times, much more symmetric than in the CBL and the smoke case. Making again the analogy with the previous cases, this can be explained by recalling that the stratocumulus topped boundary layer can be seen as a combination of the CBL and the smoke case. The plume shape in stratocumulus seems to resemble the one from the smoke cloud the most however.

Perhaps the most striking observation in figure 3 is the extremely slow plume evolution in the shallow cumulus case. This is especially surprising regarding the skewness of the top-hat velocity distribution in a cumulus cloud layer that is often assumed. We will come back to this issue in section 3.5.

3.2 *Statistics of dispersion in the CBL*

3.2.1 VERTICAL DISPERSION

The first, second and third order statistical moments and the height of maximum concentration as defined in the previous section have been plotted as a function of the dimensionless time in figure 4 for three different release heights.

The three different release heights have been chosen to cover the a large part of the boundary layer, in order to observe how the dispersion characteristics change with height. The height of maximum concentration has not been plotted for the full range, since this quantity makes no sense if we approach a vertically homogeneous particle distribution. In the mean plume height and especially the location of the maximum we see the characteristics as described in the introduction: near ground release results in a steeply rising plume, whereas elevated release results in a descending plume. The initial skewness (only shown for release at $0.5z_i$) of the plume reflects the skewness in the vertical velocity distribution. A vertically homogeneous distribution is reached for all releases after approximately $t_* = 4$. This well mixed situation is characterized by three conditions: the mean plume height is approximately half the boundary layer height $\overline{z} \approx 0.5z_i$, secondly the vertical dispersion coefficient approaches the limit $\sigma_z = 1/\sqrt{12} \approx 0.3$ and finally the skewness of the plume should approach zero: $S_z \approx 0$. The results are in satisfactory agreement with other numerical studies by Nieuwstadt (1992) and Dosio and Vilà-Guerau de Arellano (2006), who in turn validated

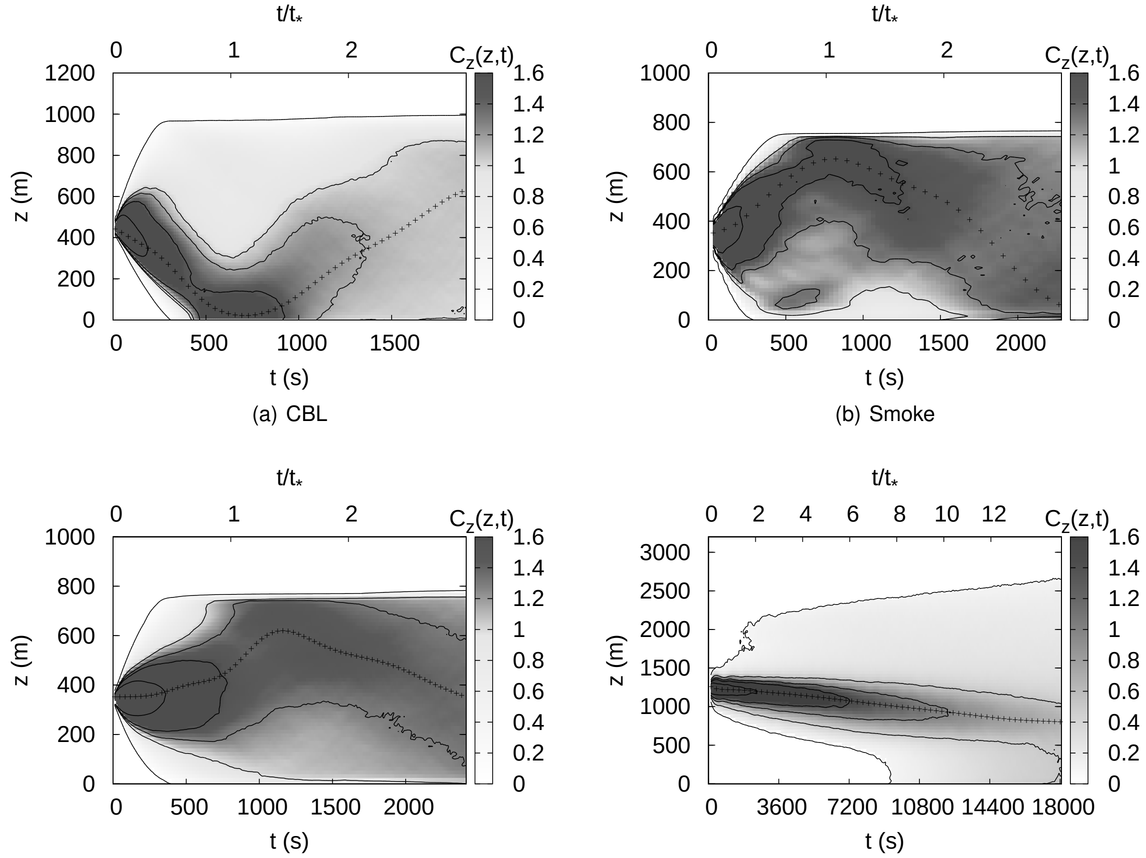

(a) CBL (b) Smoke

(c) Stratocumulus (d) Cumulus

FIG. 3: Plume evolution in four different boundary layers. A plane of particles has been released instantaneously at half the boundary layer height and the time evolution of the vertical concentration profile $C_z(z,t)$ as defined in 9 has been plotted. The concentration profile has been multiplied by 1000 to obtain a convenient scale. The points represent the location of the maximum concentration.

their results with experimental data from e.g. Willis and Deardorff (1978).

3.2.2 HORIZONTAL DISPERSION

In figure 5, the horizontal concentration profile according to equation 10 of a collection of line sources is shown. The horizontal particle distribution has a Gaussian shape, comparable to the results by Dosio and Vilà-Guerau de Arellano (2006). As they demonstrate, a simple Gaussian parametrization describes the observed plume behaviour very well. In anticipation of the results presented in the next sections, we can already say that for the horizontal dispersion in other types of boundary layers, we found the same Gaussian shaped distributions as in the CBL. In the remainder of this article we will therefore no longer focus on horizontal dispersion.

3.2.3 VERTICAL VELOCITY STATISTICS

The distribution of vertical velocity in the CBL was in the the previous section supposed to be positively skewed. In figure 6(top), the PDF of vertical velocity of the Lagrangian particles has been plotted and has the supposed positively skewed distribution. This PDF is based on particles released homogeneously in the entire CBL, so it represents the velocity distribution in the entire CBL rather than at a specific height. The Lagrangian autocorrelations of vertical velocity for particles released at three different heights has also been plotted in figure 6(bottom). The autocorrelations are in agreement with the ones found by Dosio et al. (2005).

We conclude that the dispersion results and the velocity statistics of the CBL are in satisfactory agreement with the literature. We shall therefore treat it as a reference case in understanding the results of the other cases.

3.3 ***Statistics of dispersion in the smoke cloud boundary layer***

3.3.1 VERTICAL DISPERSION

In figure 7 the dispersion characteristics for the smoke cloud boundary layer are shown. As already mentioned previously, since the smoke cloud boundary layer can be regarded a mirror-image of the CBL, we see this di-

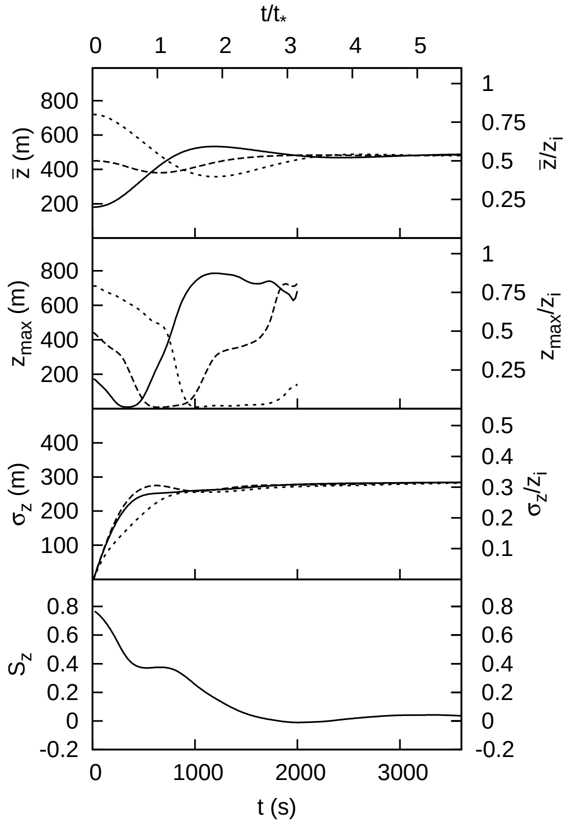

FIG. 4: From top to bottom: mean plume height, height of maximum concentration level, dispersion coefficient and skewness (only for release at $0.5z_i$) at different release levels for the dry convective boundary layer.

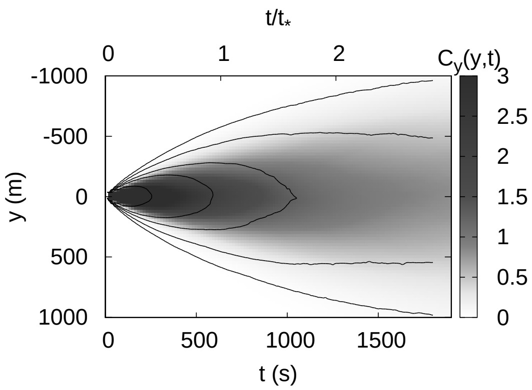

FIG. 5: Horizontal plume evolution in the CBL. In the horizontal direction the plume has a Gaussian shape.

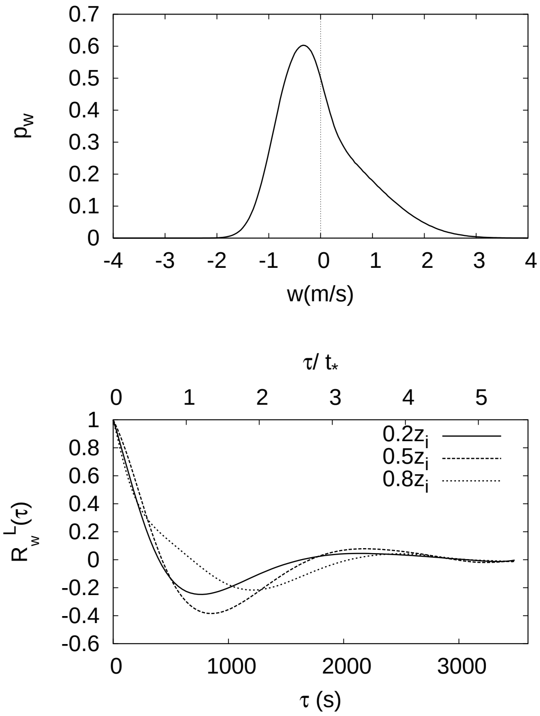

FIG. 6: Velocity distribution and autocorrelation for the CBL

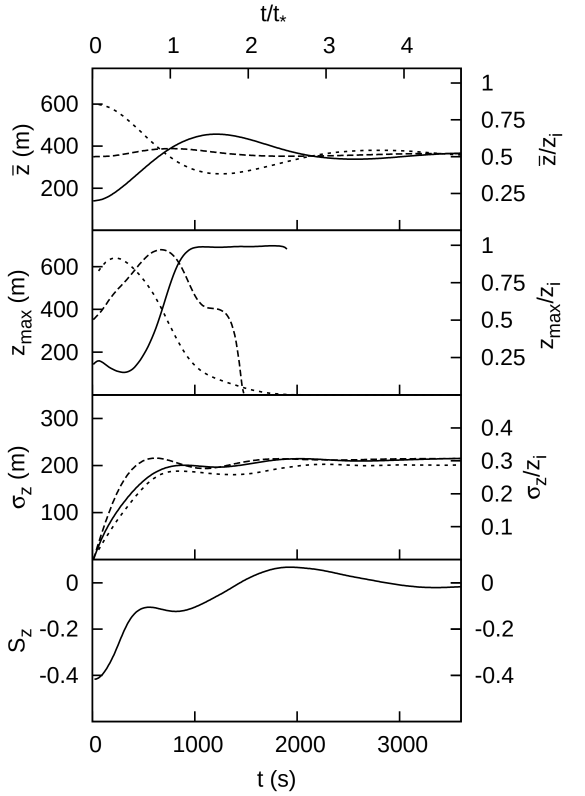

FIG. 7: From top to bottom: mean plume height, height of maximum concentration level, dispersion coefficient and skewness (only for release at $0.5z_i$) at different release levels for the smoke case.

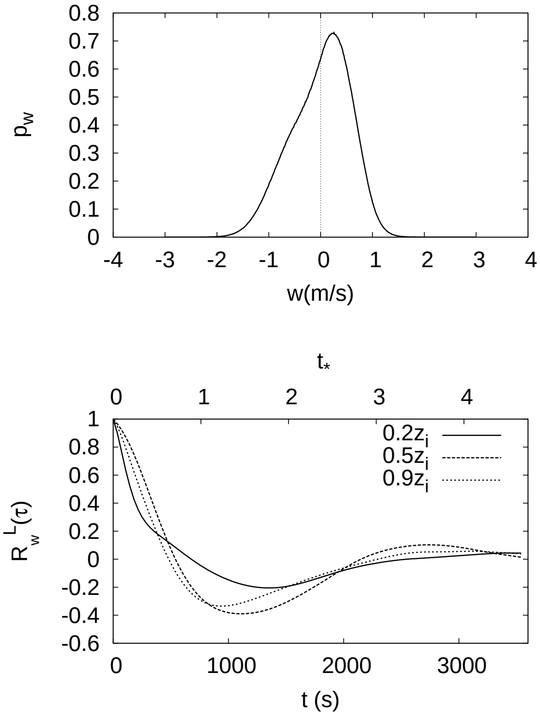

FIG. 8: Velocity distribution and autocorrelation for the smoke case

rectly in the dispersion characteristics. Considering the release at half the boundary layer height, where in the CBL the plume initially descends and impinges to the ground, in the smoke case the plume maximum rises till it reaches the capping inversion. Furthermore, we observe that a well-mixed distribution of particles ($\sigma_z \approx 0.3$) is reached after approximately the same time as in the CBL. The skewness of the plume is again a nice upside-down version of the one in the CBL, although it is somewhat smaller in magnitude. Another feature that needs to be addressed is the following: the mean plume height from the release at $0.5z_i$ seems to ascend for a while. This is at first sight rather peculiar, since a mass balance over a horizontal plane is zero by conservation of mass, thus we would expect the mean plume height to remain constant. However, we must realise that the highest velocities are found in downdrafts and hence the particles that were initially in the strongest downdrafts already impinged to the ground while the majority of particles is still in a slow updraft halfway to the inversion. The fast moving descending particles can thus only 'compensate' for the slow moving rising particles as long as they have not hit the ground yet. Indeed, a closer look shows that for very short times, the mean plume height is constant.

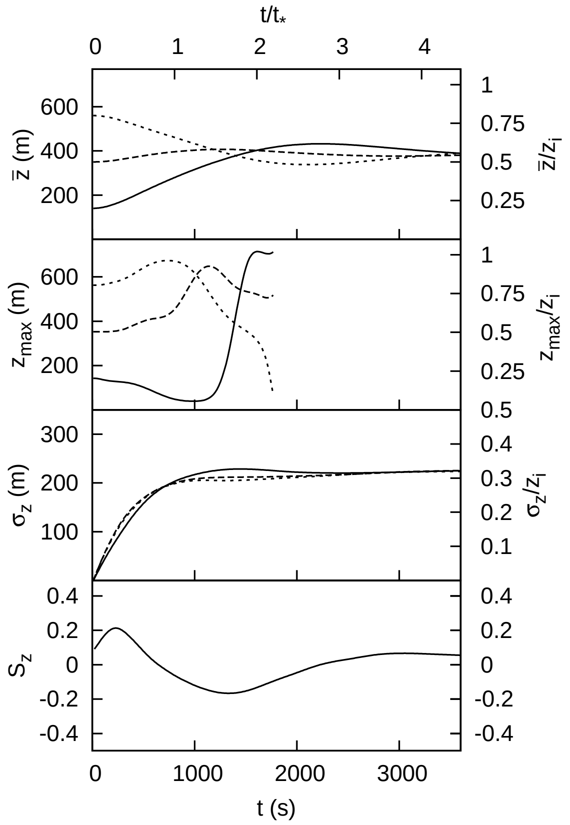

FIG. 9: From top to bottom: mean plume height, height of maximum concentration level, dispersion coefficient and skewness (only for release at $0.5z_i$) at different release levels for the stratocumulus case.

3.3.2 VELOCITY STATISTICS

Figure 8 shows the vertical velocity distribution and the Lagrangian autocorrelation of vertical velocity in the smoke cloud boundary layer. As expected, again we observe the reversed symmetry of the smoke case with the CBL, although the velocity distribution is a bit narrower. The fact that we find here the same symmetry is not surprising, since the velocity statistics obviously determine the dispersion statistics. Concerning the autocorrelations, we observe again close agreement with the CBL. The autocorrelation becomes negative because of the circular motions that many particles undergo: they first reach the capping inversion where they cannot go any further and are then caught in a downdraft. Here it is the line from the particles released closest to the ground that differs from the others, whereas in the CBL it is the line from the highest release.

We conclude from the dispersion results in the smoke case that they can be understood in the light of the vertical velocity distribution in analogy with the CBL. Furthermore, also in the purely radiatively driven smoke case, i.e. in the absence of insolation to generate a surface heat flux, rapid mixing throughout the boundary layer is observed.

3.4 *Statistics of dispersion in the stratocumulus topped boundary layer*

3.4.1 VERTICAL DISPERSION

The statistical moments of the plume evolution in the stratocumulus case have been plotted in figure 9. We repeat here that the stratocumulus topped boundary layer can be regarded as a combination of the CBL and the smoke case, for it has both the surface flux characteristic for the CBL and radiative cooling at cloud top, like the smoke cloud. This is reflected partially in the dispersion characteristics, especially in the skewness of the plume, which is, although initially positive, much closer to zero than in the previous two cases, indicating a more symmetric plume evolution. The mean plume height and height of maximum concentration are more similar to the ones found in the smoke case though. Interestingly, a close inspection of figure 9 shows that for the release at $z = 0.1z_i$ the plume maximum descends to the ground before rising again and the release in the cloud layer does the opposite. This can possibly be explained by the vertical profile being dominated by the positive surface buoyancy flux. As we mentioned earlier, the subcloud layer has a flux profile similar to the CBL, whereas the cloud layer looks more like the smoke case. de Roode and Duynkerke (1997) also noted that this leads to a skewness of the velocity distribution that changes with height: negatively skewed, i.e. stronger downdrafts in the cloud layer and positively skewed in the subcloud layer. This might explain the observed location of the plume maximum. After $t \approx 3t_*$ the particles are spread homogeneously in the vertical direction, comparable to the CBL and smoke case albeit a bit sooner than in the latter cases. We emphasize again that this result is contradicting simple dispersion models in which the dispersion parameter depends on the amount of insolation. A stratocumulus topped boundary layer has a cloud cover close to unity, so would according to these models have a dispersion coefficient that can be almost an order of magnitude lower than in the CBL. Apparently, only considering the amount of insolation is insufficient to describe the dispersion in a cloudy boundary layer like the stratocumulus case.

3.4.2 VELOCITY STATISTICS

In figure 10, the velocity statistics from the stratocumulus case have been plotted. The velocity distribution is much more symmetric than in the previous cases, and is in agreement with the characteristics of the plume. The autocorrelations very much resemble the ones from the CBL and the smoke case. The autocorrelation of the particles released in the top of the cloud layer has a shape similar to the one in the smoke case, again confirming that the stratocumulus cloud layer has the same characteristics as the smoke cloud. It should be mentioned that in the stratocumulus case considered here the cloud layer and the sub-cloud layer were coupled, as was clear from the velocity variance profile (not shown here). One could argue that dispersion in a decoupled stratocumulus topped boundary layer has different dispersion characteristics.

3.5 ***Statistics of dispersion in the cumulus topped boundary layer***

3.5.1 VERTICAL DISPERSION

In the cumulus case we make a clear distinction between release in the sub-cloud layer and release in the cloud layer.

From figure 3(d) it was already clear that dispersion in the cumulus cloud layer was very different than in the other cases. It is instructive to look at the plume evolution in another way than the contourplot from figure 3. Figure 12 shows the vertical distribution of particles released in the sub-cloud layer (bottom) and in the cloud-layer (top) at different times. Figure 11 shows the statistical moments of the plume evolution. Referring to figure 12, it can be seen that release in the sub-cloud layer shows that dispersion in the sub-cloud layer is analogous to the CBL: initially the plume maximum descends to the ground and then rises again. We also observe this in figure 11, although the location of the plume maximum has only been plotted for short times for release in the sub-cloud layer, because in a well mixed situation this quantity looses its relevance. After 30 minutes we observe a vertically well mixed profile in the sub-cloud layer, but clouds have transported a small part of the particles into the cloud layer. Clouds continue to bring particles upwards, so the concentration in the sub-cloud layer slowly decreases in time (cloud venting), whereas the number of particles in the cloud layer grows. These observations are in agreement with Vilà-Guerau de Arellano et al. (2005), although they did not observe the diminishing concentration in the sub-cloud layer since they prescribed a continuous surface flux of pollutants. The effect of cloud venting can also be seen in figure 11, where we see a steadily increasing dispersion coefficient for the release in the sub-cloud layer. One could speculate that this dispersion coefficient is made of two components: one from the dispersion in the sub-cloud layer, which is constant after approximately 30 minutes and one from the effect of cloud venting, which has a much larger time-scale.

Next we consider the release in the cloud layer. The plume is positively skewed, also observed in the bottom graph of figure 11, which reflects the skewed velocity distribution in the cloud layer. Nonetheless, looking at the height of the maximum concentration, we observe that it descends only very slowly, unlike we would expect from the analogy with the CBL. Moreover, the dispersion parameter shows that the plume spreads much slower in the cumulus cloud layer than in all other cases, not only in absolute sense (the dispersion coefficient measured in meters), but also in dimensionless units. In the other cases, a vertically well mixed concentration profile was reached after $t \sim 3t_*$; in the cumulus cloud layer this is not even the case after $t \sim 8t_*$. It is interesting to combine the information that both graphs in figure 12 provide

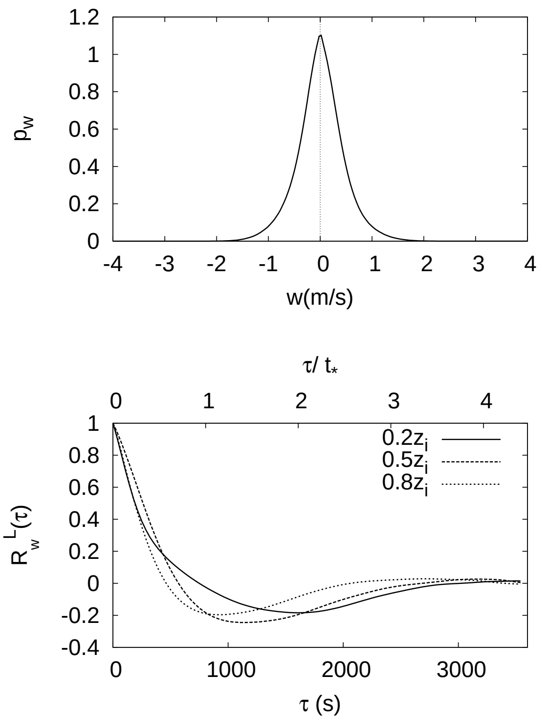

FIG. 10: Velocity distribution and Lagrangian autocorrelation for the stratocumulus topped boundary layer

to sketch the following conceptual picture: Clouds transport particles (pollutants) from ground level to the cloud layer, where they detrain from the cloud into the stable environment where they hardly move anymore – a phenomenon sometimes referred to as plume trapping. We emphasize that this result is rather surprising and cannot be understood in the light of the classical view on vertical transport by cumulus clouds, i.e. strong narrow updrafts in cloudy regions surrounded by homogeneously distributed downdrafts. The latter motions would transport the pollutants to cloud-base in a steady pace. The velocity statistics shed more light on this issue.

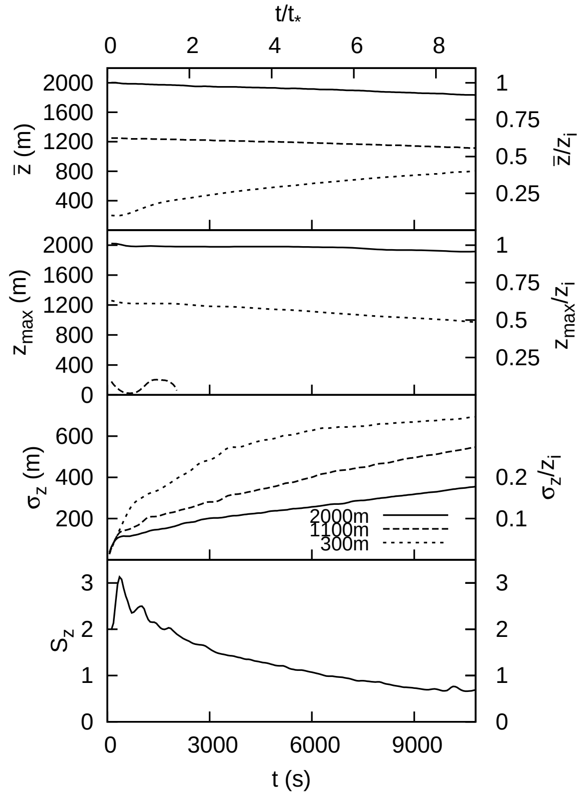

FIG. 11: Mean plume height, height of maximum concentration level, vertical dispersion coefficient and skewness (only for release at 1100m) at different release levels for the shallow cumulus topped boundary layer. Note that cloudbase is approximately at $0.25z_i$

3.5.2 VELOCITY STATISTICS

The distribution of vertical velocity in the cumulus cloud layer is shown in figure 13 together with a twodimensional velocity distribution, where the new coordinate r represents the distance to the nearest cloud, equivalent to Jonker et al. (2008). Negative values for r are locations inside the cloud. The figure shows that indeed particles in a cloud move mostly upward, particles near a cloud move mostly downward, whereas in the far environment particles have zero average velocity, although the variance of the velocity is clearly not zero. Nevertheless, this still does not explain why particles spread so slowly in the cumulus cloud layer, because, after all, the velocity distribution in the stratocumulus topped boundary layer is not so much different than in the cumulus cloud layer. To understand this we invoke the autocorrelation functions from figure 14. The autocorrelation of the particles released in the sub-cloud layer very much resembles the ones in the CBL, which is expected because the subcloud layer has all the characteristics of a CBL. For release in the cloudlayer, there seems to be wavelike component in the autocorrelation function. Recalling that the cloud layer in a cumulus field is stratified for dry air, we can expect the presence of buoyancy waves, as is also shown in a theoretical analysis for stable boundary layers by Csanady (1973). The frequency of these oscillations, the Brunt-Väisälä frequency, is given by

$$\omega = 2\pi\sqrt{\frac{g}{\theta}\frac{d\theta}{dz}} \qquad (12)$$

One could argue that the autocorrelation of the vertical velocity in a stratified medium is made of two components: one from stochastic motion associated with turbulence and one from the wavelike motion associated with buoyancy waves. Mathematically this would then translate to

$$R^L(\tau) = e^{-\left(\frac{\tau}{T^L}\right)}\cos(\omega t) \qquad (13)$$

where T^L is then some characteristic timescale over which the turbulent velocity is correlated. If the suggestion of buoyancy waves is indeed true, then ω in equation 13 should correspond with 12. To verify this we computed the autocorrelations for many different release heights, fitted the results with equation 13 and so obtained a vertical profile of T^L and ω. From the LES fields we have the virtual temperature profiles, thereby allowing us to make a vertical profile of equation 12. Figure 15 shows the results. The values of ω as fitted from the autocorrelations correspond reasonably well with the ones calculated from the Brunt-Väisälä frequency.

The view that emanates from the above considerations is that the vast majority of particles in the cumulus cloud layer is just lingering in the environment, every now and then get disturbed from their vertical position when a cloud 'kicks' the whole system and will then start to oscillate for a while around its original position. This explains why we do find a velocity distribution with a reasonable velocity variance, but yet hardly observe any plume spreading. The effective transport of pollutants is done solely by the cloud and the surrounding subsiding shell. The rather surprising conclusion from this view is that particles not only need a cloud to go up, but also to go down.

4. CONCLUSIONS

We investigated the dispersion characteristics in different types of boundary layers in an LES based study together

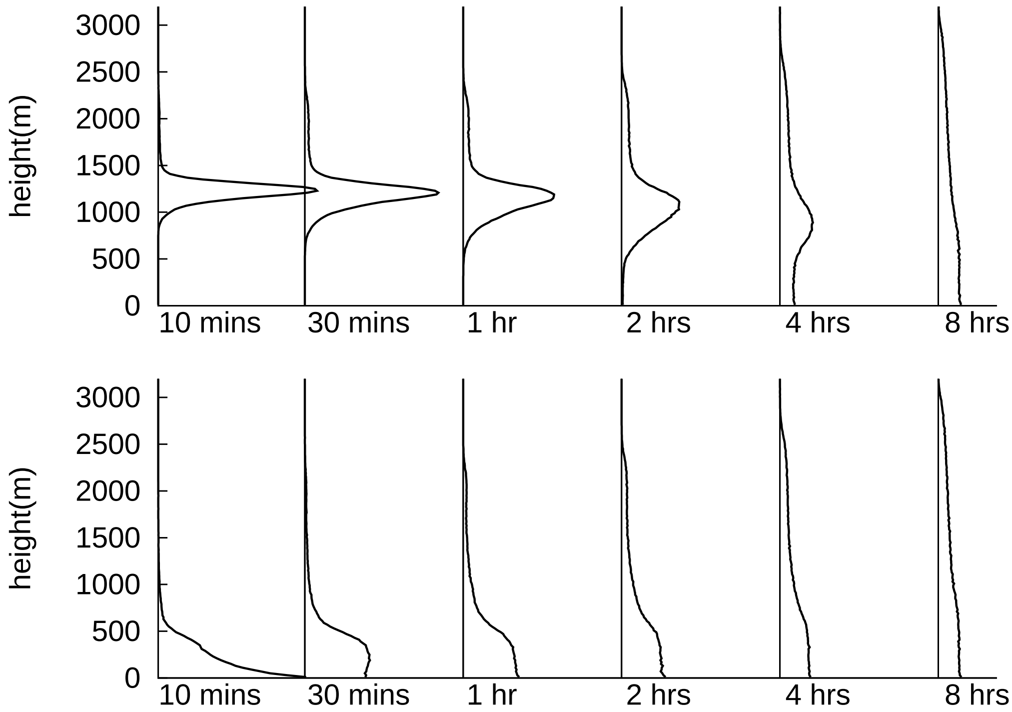

FIG. 12: Time evolution of the vertical concentration profile for the cumulus case. Bottom: release in the subcloud layer (200 m). Top: release in the cloud layer (1250 m).

with a Lagrangian particle dispersion module. Comparison with the extensively documented dispersion in the dry convective boundary layer showed satisfactory agreement with the literature and can be explained from the skewness of the velocity distribution.

The vertical dispersion results from the smoke case and the stratocumulus case can be fully understood in terms of the vertical velocity distribution in the boundary layer. With the CBL as a reference case, the smoke case has the opposite velocity distribution and hence also mirrored dispersion characteristics. Radiative cooling at the top of the smoke cloud leads to strong narrow downdrafts and compensating updrafts. This negatively skewed velocity distribution translates into an initially rising plume maximum.

The stratocumulus case can best be viewed as combination of the smoke case and the CBL. The cloud layer, where radiative cooling is dominant, resembles the smoke case the most, whereas the sub-cloud layer, where the surface fluxes dominate, looks more like the CBL. A study of dispersion in a decoupled stratocumulus case would be interesting to pursue.

Future parametrizations of vertical dispersion in the smoke case and the stratocumulus case should exploit the symmetry with respect to the CBL, where parametrization have already been proposed and validated.

It should be emphasized that in both the smoke case and the stratocumulus case we observe rapid mixing throughout the boundary layer. This observation contradicts simple dispersion models in which clouds have a damping effect on dispersion by blocking insolation.

The shallow cumulus case shows markedly different dispersion characteristics. First of all, we observe cloud venting: clouds transport particles from the sub-cloud layer upwards. Secondly, dispersion in the cloud layer is much slower than in all other cases and as anticipated solely on the basis of the velocity distribution. It turns out that the velocity distribution as a function of distance to cloud and the vertical velocity autocorrelations need to be invoked to understand the observations. By doing so, the view that emanates is that particles far away from clouds display oscillating behaviour associated with buoyancy waves. This results in a velocity distribution with a variance comparable to the other three cases, but yet a very slow spreading of the plume. The overall picture that emerges is that clouds deposit pollutants emitted at ground level in the cloud layer, where they remain for very long times.

This view has consequences for the concentration variance in the cloud layer. Since pollutants in the environment far away from clouds mix very slowly throughout the cloud layer, there will remain areas with high concentrations for relatively long times. This might have consequences for chemical processes that are often non-linear with respect to the concentrations of the reactants.

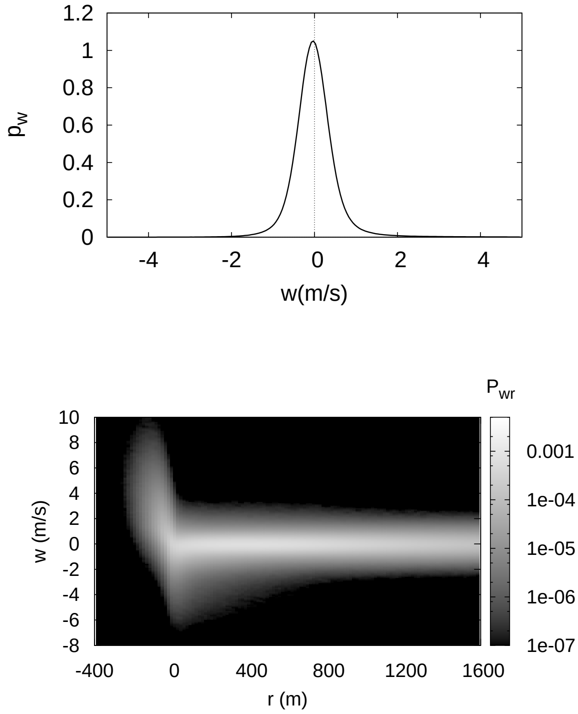

FIG. 13: Vertical velocity distribution in the cumulus cloud layer (top) and vertical velocity distribution as a function of distance to cloud (bottom).

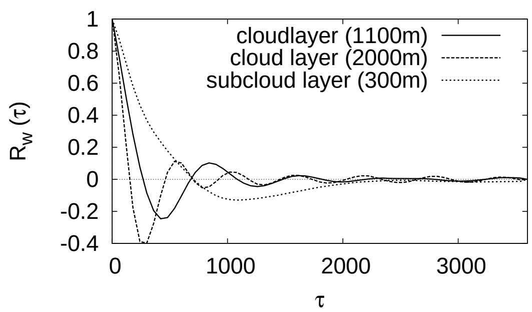

FIG. 14: Vertical velocity autocorrelation in the cumulus case

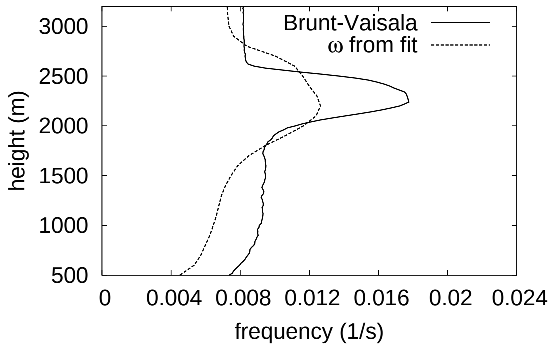

FIG. 15: Comparison between profiles of the Brunt-Väisälä frequency as calculated by Eq. 12 and the values of ω obtained by fitting Eq. 13 to the Lagrangian autocorrelations from different rellease heights.

ACKNOWLEDGMENTS

The authors thank Jordi Vilà-Guerau de Arellano for stimulating discussions and suggestions. This work was sponsored by the Stichting Nationale Computerfaciliteiten (National Computing Facilities Foundation, NCF), with financial support from the Nederlandse Organisatie voor Wetenschappelijk Onderzoek (Netherlands Organization for Scientific Research, NWO).

REFERENCES

Angevine, W. M., 2005: An integrated turbulence scheme for boundary layers with shallow cumulus applied to pollutant transport. *Journal of Applied Meteorology*, **44**(9), 1436–1452.

Bretherton, C. S., et al., 1999: An intercomparison radiatively-driven entrainment and turbulence in a smoke cloud, as simulated by different numerical models. *Quart. J. Roy. Meteor. Soc.*, **125**, 391–423.

Briggs, G., 1993: Plume dispersion in the convective boundary layer. part ii: Analyses of condors field experiment data. *Journal of Applied Meteorology*, **32**(8), 1388–1425.

Ching, J. K. S., S. T. Shipley, and E. V. Browell, 1988: Evidence for cloud venting of mixed layer ozone and aerosols. *Atmospheric Environment (1967)*, **22**(2), 225–242.

Cotton, W., 1995: Cloud venting - a review and some new global annual estimates. *Earth-Science Rev.*, **39**, 169–206.

Csanady, G., 1973: *Turbulent diffusion in the environment*. D.Reidel Publishing company.

Cuijpers, J. W. M., and P. G. Duynkerke, 1993: Large-eddy simulation of trade wind cumulus clouds. *J. Atmos. Sci.*, **50**, 3894–3908.

de Roode, S., and P. Duynkerke, 1997: Observed lagrangian transition of stratocumulus into cumulus during astex: mean state and turbulence structure. *J. Atmos. Sci.*, **54**, 2157–2173.

Deardorff, J. W., 1980: Stratocumulus-capped mixed layers derived from a three-dimensional model. *Boundary-Layer Meteorology*, **18**(4), 495–527.

Dosio, A., and J. Vilà-Guerau de Arellano, 2006: Statistics of absolute and relative dispersion in the atmospheric convective boundary layer: A large-eddy simulation study. *Journal of the Atmospheric Sciences*, **63**(4), 1253–1272.

Dosio, A., J. V. G. De Arellano, A. A. M. Holtslag, and P. J. H. Builtjes, 2005: Relating eulerian and lagrangian statistics for the turbulent dispersion in the atmospheric convective boundary layer. *J. Atmos. Sci.*, **62**(4), 1175–1191.

Heus, T., and H. J. J. Jonker, 2008: Subsiding shells around shallow cumulus clouds. *Journal Of The Atmospheric Sciences*, **65**(3), 1003–1018.

Heus, T., G. van Dijk, H. J. J. Jonker, and H. E. A. van den Akker, 2008: An les-based study on the shallow cumulus cloud mixing controversy. *J. Atmos. Sci.*. In press.

Hundsdorfer, W., B. Koren, M. Vanloon, and J. G. Verwer, 1995: A positive finite-difference advection scheme. *J. Comput. Phys.*, **117**(1), 35–46.

Jonker, H. J. J., T. Heus, and P. P. Sullivan, 2008: A refined view of vertical mass transport by cumulus convection. *Geophysical Research Letters*, **35**(7), L07,810.

Lamb, R. G., 1978: A numerical simulation of dispersion from an elevated point source in the convective planetary boundary layer. *Atmospheric Environment (1967)*, **12**(6-7), 1297–1304.

Neggers, R. A. J., H. J. J. Jonker, and A. P. Siebesma, 2003: Size statistics of cumulus cloud populations in large-eddy simulations. *J. Atmos. Sci.*, **60**(8), 1060–1074.

Nieuwstadt, F. T. M., 1992: A large-eddy simulation of a line source in a convective atmospheric boundary layer–i. dispersion characteristics. *Atmospheric Environment. Part A. General Topics*, **26**(3), 485–495.

Pasquill, F., 1961: The estimation of the dispersion of windborne material. *Meteor. Mag.*, **90**, 33–49.

Siebesma, A. P., and J. W. M. Cuijpers, 1995: Evaluation of parametric assumptions for shallow cumulus convection. *J. Atmos. Sci.*, **52**(6), 650–666.

Taylor, G., 1921: Diffusion by continuous movements. *Proc.London Math. Soc.*, **20**, 196–212.

Thomson, D. J., 1987: Criteria for the selection of stochastic models of particle trajectories in turbulent flows. *J. Fluid Mech.*, **180**, 529–556.

Vilà-Guerau de Arellano, J., S.-W. Kim, M. C. Barth, and E. G. Patton, 2005: Transport and chemical transformations influenced by shallow cumulus over land. *Atmos. Chem. Phys.*, **5**(12), 3219–3231.

Weil, J., E. Patton, and P. Sullivan, 2006: Lagrangian modeling of dispersion in the stable boundary layer. *17th Symposium on Boundary Layers and Turbulence, 2006*.

Weil, J. C., R. P. Lawson, and A. R. Rodi, 1993: Relative dispersion of ice crystals in seeded cumuli. *Journal of Applied Meteorology*, **32**(6), 1055–1073.

Weil, J. C., P. P. Sullivan, and C. H. Moeng, 2004: The use of large-eddy simulations in lagrangian particle dispersion models. *J. Atmos. Sci.*, **61**(23), 2877–2887.

Willis, G. E., and J. W. Deardorff, 1978: A laboratory study of dispersion from an elevated source within a modeled convective planetary boundary layer. *Atmospheric Environment (1967)*, **12**(6-7), 1305–1311.